Available online at www.sciencedirect.com

SciVerse ScienceDirect

Ceramics International 39 (2013) 4929–4936

CERAMICS INTERNATIONAL

www.elsevier.com/locate/ceramint

Influence of Fe^{3+}-doping on optical properties of CeO_{2-y} nanopowders

M. Radović[a], Z. Dohčević-Mitrović[a,*], A. Golubović[a], V. Fruth[b], S. Preda[b], M. Šćepanović[a], Z.V. Popović[a]

[a]Center for Solid State Physics and New Materials, Institute of Physics, University of Belgrade, Pregrevica 118, 11080 Belgrade, Serbia
[b]Institute of Physical Chemistry "Ilie Murgulescu", Romanian Academy, 202 Splaiul Independentei, 060021 Bucharest, Romania

Received 12 October 2012; received in revised form 19 November 2012; accepted 26 November 2012
Available online 3 December 2012

Abstract

$Ce_{1-x}Fe_xO_{2-y}$ ($0 \le x \le 0.05$) nanopowders were synthesized using hydrothermal method at low calcination temperature and low doping regime. Structural and morphological characterization has been carried out by the X-ray diffraction method and non-contact atomic force microscopy. Vibrational properties were investigated by Raman spectroscopy. It was observed that the content of oxygen vacancies increased significantly with Fe doping up to 3 mol%. For higher dopant concentration, phase separation was detected. The optical properties of pure and Fe^{3+}-doped CeO_{2-y} samples were investigated by spectroscopic ellipsometry. Several analytical models were applied to analyze the optical absorption onset of ceria defective structure. It was found that, Cody–Lorentz model most suitably described the sub-band gap region of CeO_{2-y} nanopowders and consequently gave more accurate band gap values, which are closer to the direct band gap transitions than to the indirect ones. The increased content of localized defect states in the ceria gap and corresponding shift of the optical absorption edge towards visible range in Fe-doped samples can significantly improve the optical activity of nanocrystalline ceria.

Keywords: A. Powders: chemical preparation; B. Spectroscopy; C. Optical properties; D. CeO_2

1. Introduction

Ceramic materials based on cerium oxide (ceria, CeO_2) have been a very active research field in the area of photocatalytic technologies such as production of oxygen trough water decomposition [1] and photodegradation of toluene in gas phase [2], methylene blue [3], acidic black 10b [4] and acid orange 7 [5] industrial dyes. The recent study of Ji et al. [5] have revealed that nanophased CeO_2 is more efficient photocatalyst in the visible region for dye wastewater treatment than the commercial TiO_2 [5]. Doping with transition metals, such as Fe, enhances the oxygen mobility and oxygen storage capacity of ceria lattice [6] which can improve photocatalytic properties of CeO_2 nanomaterials [3]. Also Fe-doped ceria nanoparticles were used for pigmented ultraviolet filter applications [7]. The optimization of photocatalytic technologies which utilize solar radiation is directed towards the development of ceria materials with precisely controlled position of the absorption edge and tunable electronic band structure.

Even though extensive research has been performed on the optical properties of ceria based nanomaterials, still a lot of controversy exists in the literature regarding the nature of the optical band gap transition (E_g) which corresponds to the O 2p→Ce 4f transition. Guo et al. [8] reported the optical band gap values of 3.6 eV and 3.3 eV for direct and indirect transitions respectively, in a case of bulk (crystalline film) ceria sample. A certain number of authors [9–12] have calculated the optical band gap of various ceria based materials, treating it as a direct transition. Contrary to them, a group of other authors [13–17] ascribed the optical band gap of CeO_2 to the indirect transition. Independent measurements performed on oxygen deficient ceria structures using non optical techniques, gave the values of 3.3 eV [18], and 3.4–3.6 eV

*Corresponding author. Tel.: +381 11 3713024; fax: +381 11 3162190.
E-mail address: zordoh@ipb.ac.rs (Z. Dohčević-Mitrović).

0272-8842/$ - see front matter © 2012 Elsevier Ltd and Techna Group S.r.l. All rights reserved.
http://dx.doi.org/10.1016/j.ceramint.2012.11.087

[19] without defining the type of the transition. The present uncertainty in the band gap calculations of nanostructured CeO_{2-y} increases a need for better explanation of its electronic properties using sophisticated analytical models which incorporate nanosized ceria defective structure.

The decrease of the particle size to nanodimensions leads to the increase of the band gap energy in majority of materials due to the quantum confinement effects [20]. In a case of nanoceria an anomalous behavior in the band gap energy was observed for the grain size less than 20 nm [9]. The decrease of the band gap energy with grain size decrease can be explained by a transformation from the crystalline into the amorphous state when crystals become of nanodimension [9] and increase in the number of defects within the band gap [16]. All these nano-size related effects are reflected in the spectral dependence of the complex dielectric function which is, through its imaginary part ($\varepsilon_2(E)$), related to the energy-band structure. Being a nondestructive and very sensitive technique, spectroscopic ellipsometry (SE) represents a very convenient method for precise and direct determination of the complex dielectric function of nanostructured materials from which important information about materials electronic structure can be obtained.

The aim of this work was to investigate the influence of Fe^{3+}-doping on the optical properties and band gap behavior of CeO_{2-y} nanopowders. We applied different ellipsometric models in order to deduce which model describes best the electronic properties of nonstoichiometric pure and Fe^{3+}-doped CeO_{2-y}.

2. Experiment

Non-stoichiometric nanopowders of pure CeO_{2-y} (coefficient y denotes the oxygen deficiency and for small particles ranges from 0–0.2 [21,22]) and CeO_{2-y} doped with 1 mol%, 3 mol% and 5 mol% of trivalent iron ions were synthesized by the hydrothermal method using NH_4OH solution and relatively low calcination temperature (200 °C). Detailed preparation procedure is published elsewhere [23].

The X-ray diffraction (XRD) patterns were collected using Rigaku RINT2200 powder diffractometer. Non-contact atomic force microscopy (NC-AFM) microscopy measurements were carried out using Omicron B002645 SPM probe VT AFM 25. Micro-Raman scattering measurements were performed at room temperature using a Jobin-Yvon T64000 triple spectrometer system equipped with a liquid-nitrogen cooled CCD detector. The $\lambda=514.5$ nm line of an Ar^+/Kr^+ mixed laser was used as an excitation source. The ellipsometric measurements were performed at $\theta_i=70^\circ$ incidence angle in the UV–Vis spectral range, using high resolution variable angle spectroscopic ellipsometer (SOPRA GES5E-IRSE) of the rotating polarizer type.

3. Analytical models

From the measurements of ellipsometric angles Ψ and Δ, by using the two-phase model approximation (CeO_{2-y} nanoparticles/air), we have calculated the pseudo-dielectric function spectra directly from the complex reflectance ratio $\rho(E)=\tan\Psi\exp(i\Delta)$ using the relation [24]

$$\langle\varepsilon(E)\rangle=\sin^2\theta_i\left[1+tg^2\theta_i\left(\frac{1-\rho(E)}{1+\rho(E)}\right)^2\right], \quad (1)$$

where θ_i is the incidence angle. Measurement of pseudo-dielectric function enables direct determination of real and imaginary part of the complex dielectric function spectrum $\varepsilon(E)=\varepsilon_1(E)+i\varepsilon_2(E)$. The imaginary part of complex dielectric function ($\varepsilon_2(E)$) can provide useful information about the electronic density of states and the band structure of the investigated material.

One of the most frequently used, but oversimplified models for the band gap calculations from optical measurements, was developed by Tauc et.al. [25]. A general expression for $\varepsilon_2(E)$ is derived under the assumption of parabolic density of states, constant momentum matrix element and relaxed selection rules for direct and indirect transitions, respectively

$$\left(\varepsilon_2\cdot E^2\right)^2=a\left(E-E_g\right), \quad (2a)$$

$$\sqrt{\varepsilon_2}\cdot E=b\left(E-E_g\right), \quad (2b)$$

where E is the photon energy, E_g is the band gap and constants a and b are related to the density of states in conduction band. This model is often known in the literature as Tauc law.

Aiming to obtain the value of the band gap and at the same time to take into account the interband electronic transitions Jellison and Modine [26] derived a model for the $\varepsilon_2(E)$ on the basis of the Tauc law and Lorentz oscillator model, expressed as

$$\varepsilon_2(E)=\begin{cases}0, & E\le E_g;\\ \frac{\left(E-E_g\right)^2}{E^2}\cdot\frac{AE_0\Gamma E}{\left(E^2-E_0^2\right)^2+\Gamma^2E^2} & E>E_g;\end{cases} \quad (3)$$

where A, E_0, and Γ are the peak amplitude, position and width, respectively. This model is known as the Tauc–Lorentz (TL) model and is based on the assumption of parabolic density of states and constant momentum matrix element.

Better results for the absorption onset behavior in amorphous silicon hydride films were obtained by Cody et al. [27] who applied constant dipole matrix element instead of constant momentum matrix element, but significant improvement of the TL and Cody's models was demonstrated by Ferlauto et.al. [28]. In the region bellow the band edge, Ferlauto and co-workers, used Urbach rule to describe the behavior of dielectric function of amorphous (disordered) materials. According to this rule,

Urbach tails are usually observed as an exponential increase of absorption in the bellow band gap region. The absorption coefficient can be described as [29]

$$\alpha(E,T)=\alpha_0\exp\left(\frac{\sigma(E-E_0)}{kT}\right) \quad (4)$$

where α_0 and E_0 are material parameters, σ is steepness parameter and k is Boltzman constant. The Urbach energy, defined as $E_U=kT/\sigma$, indicates the width of the band tails of the localized states.

Ferlauto and coworkers also introduced a modification of Cody's model and presented an alternative expression for the dielectric function just above the optical absorption edge

$$\varepsilon_2 \propto \frac{(E-E_g)^2}{(E-E_g)^2+E_p}, \quad (5)$$

The model, known in the literature as Urbach–Cody–Lorentz (UCL) model or just Cody–Lorentz (CL) model, can be expressed as

$$\varepsilon_2(E)=\begin{cases}\dfrac{E_1}{E}\exp\left\{\dfrac{(E-E_t)}{E_u}\right\}; & 0<E\le E_t;\\ \dfrac{(E-E_g)^2}{(E-E_g)^2+E_p^2}\cdot\dfrac{AE_0\Gamma E}{(E^2-E_0^2)^2+\Gamma^2E^2}; & E>E_t,\end{cases} \quad (6)$$

where parameter E_c ensures continuality of dielectric function at $E=E_t$, E_t is the demarcation energy between Urbach tail region and interband transitions. The energy E_p separates the absorption onset behavior from the Lorentz oscillator behavior, giving to this expression more flexibility in the numerical modeling.

It is worth mentioning that TL and CL models do not take into account the nature of optical transition and can be applied for both, direct and indirect band gap type of materials.

4. Results and discussion

In Fig. 1 are given the XRD spectra of pure and Fe^{3+}-doped CeO_{2-y} samples. All synthesized samples have fluorite type crystal structure of cerium dioxide and no secondary phase was detected. Characteristic Miller indices are denoted for each diffraction peak.

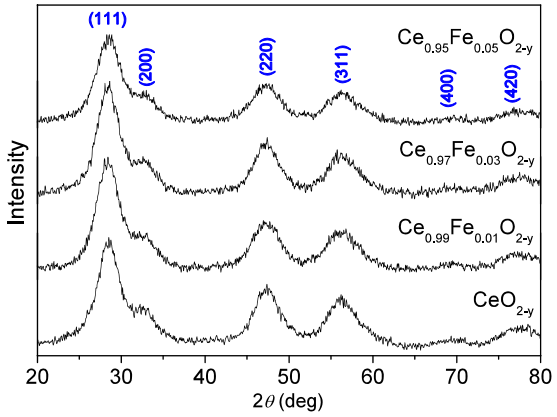

Fig. 1. XRD spectra of pure and Fe-doped CeO_{2-y} nano powders.

Significant broadening of the peaks indicates that investigated powders consist of nanometric size crystallites. The crystallite size D of the samples was estimated from XRD data by taking into account strain contribution, using the Williamson-Hall method [30]

$$\beta\cos\theta=\frac{K\lambda}{D}+4\varepsilon\sin\theta \quad (7)$$

where β is the peak width, K is the form factor (0.9 for spherical particles), λ is the radiation wavelength and ε is the strain. The crystallite size and strain can be determined from the intercept and slope of the $\beta\cos\theta$ vs $4\sin\theta$ plots. The average crystallite size of pure CeO_{2-y} nanopowder was about 4 nm, becoming smaller with increasing Fe^{3+} content. The values of average crystallite size and strain are presented in Table 1 for each sample. Slight decrease of strain with Fe doping up to 5 mol% implies that smaller Fe^{3+} ions enter substitutionary into ceria lattice replacing bigger Ce^{3+} ions.

In Fig. 2(a) are shown the Raman spectra of $Ce_{1-x}Fe_xO_{2-y}$ ($0\le x\le 0.05$) nanopowders. The baseline correction of the Raman spectra was performed by using the Bose–Einstein thermal correction and a two-point baseline correction [31]. The most prominent peak is the first order F_{2g} Raman mode, positioned at about 454 cm^{-1} in undoped CeO_{2-y} sample [32]. In doped samples the softening and broadening of this mode was observed with the increase of Fe^{3+} concentration [33]. The cause of this unexpected shift and broadening can be explained by the delocalization of unpaired Fe^{3+} electrons on Ce(Fe)–O(Vo)–Ce(Fe) orbitals and electron-molecular vibration coupling mechanism [34]. Another mode at 600 cm^{-1} corresponds to the oxygen vacancy Raman mode (V_o) characteristic for nanocrystalline CeO_{2-y} [32]. In Fig. 2(b) are shown Lorentzian lineshape fits of the V_o mode for all investigated samples. The reasonably good fits for all samples were obtained with one Lorentzian, except the 5% Fe-doped sample. In a case of $Ce_{0.95}Fe_{0.05}O_{2-y}$ sample additional mode appears at 650 cm^{-1} and the good fit of this spectrum was obtained by fitting with two Lorentzians. This mode, most probably originates from the iron oxide–wüstite (FeO) phase [35]. Although this phase was not detected in the XRD spectrum of this sample we concluded that small concentration of wüstite phase was formed on the nanoparticle surface, for which the Raman

Table 1
Average crystallite size D and microstrain ε obtained from Williamson–Hall plots of XRD data.

	CeO_{2-y}	1 mol% Fe	3 mol% Fe	5 mol% Fe
D (nm)	4.0(5)	3.1(5)	2.9(5)	2.9(5)
ε (%)	1.6(1)	1.1(2)	0.7(1)	0.9(2)

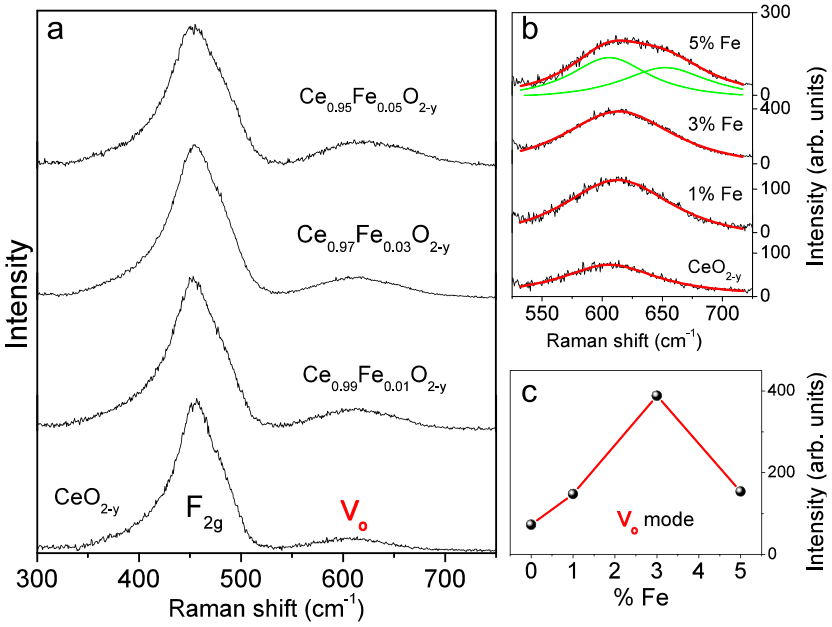

Fig. 2. (a) Raman spectra of pure and Fe doped CeO_{2-y} nanopowders, (b) Lorentzian lineshape analysis of oxygen vacancy mode, V_o and (c) intensity variation of V_o mode.

scattering method is more sensitive, and the phase separation took place. On the other hand, the formation of wüstite phase is followed by decrease of the oxygen vacancy concentration, which can be explained by the fact that Fe atoms do not enter into ceria lattice to form additional vacancies but remain in the surface layer forming iron oxide phase.

From the Lorentzian lineshape fitting of the Raman spectra we have observed that the intensity of V_o mode increases in Fe^{3+}-doped samples (Fig. 2(c)) up to the 3 mol% of Fe, as a consequence of increased oxygen vacancies concentration and afterwards decreases.

The NC-AFM images of pure, 3 mol% and 5 mol% Fe doped CeO_{2-y} samples are shown in Fig. 3(a–c), respectively. From these images we can observe that samples consist of very small nanocrystals and agglomerated particles. The topography image of the 5 mol% Fe doped sample exhibits new features that can be ascribed to phase separation [36]. The existence of grains marked with arrows in Fig. 3(c) points out to significant difference in sample topography compared to the pure and 3 mol% Fe doped samples. The obtained results are in agreement with Raman spectroscopy.

The imaginary part of the pseudo-dielectric function, $\langle \varepsilon_2(E) \rangle$, is deduced from the ellipsometric measurements, by applying two-phase model approximation, already discussed (Eq. (1)). In order to investigate the optical band gap nature and the influence of Fe dopant on the behavior of the absorption edge in ceria nanocrystals we first applied oversimplified Tauc model to determine the energies of the direct or indirect band gap transitions. In Fig. 4(a) are presented the plots of "Tauc density of states", treating pure and Fe^{3+}-doped CeO_{2-y} nanopowders as an indirect band gap material whereas in Fig. 4(b) are given the same plots in a case of direct band gap transition. The straight lines are linear fits according to Eqs. (2a) and (2b), from which band gap values are determined. The calculated values of both direct and indirect band gap values for pure nanocrystalline ceria (3.32 and 2.4 eV) were lower than the values of bulk sample (3.6 and 3.3 eV) [8]. This is characteristic for defective ceria nanostructure [9,16]. Doping with Fe^{3+} ions induces a shift of the optical absorption edge towards visible spectral range up to 5 mol% of Fe dopant. In a case of $Ce_{0.95}Fe_{0.05}O_{2-\delta}$ sample in which the phase separation was detected from the Raman spectra, the band gap value both for direct and indirect band gap transition increased.

The main disadvantages of Tauc model is that this model gives slightly overestimated band gap values in a reflection type of measurement, such as spectroscopic ellipsometry, and does not take into account the possible presence of defect states inside the gap. This is already discussed in the work of Ferlauto et al. [28]. We then applied more sophisticated TL model to analyze the $\langle \varepsilon_2(E) \rangle$ spectra of the samples.

In Fig. 5 are presented experimentally obtained spectra of $\langle \varepsilon_2(E) \rangle$ for pure and Fe doped samples (open circles) in the 1.5 to 6.5 eV region. The best fits based on TL model using Eq. (3) are presented with dashed lines. For the Lorentzian lineshape fits we have used two oscillators to describe the peaks observed in the dielectric function spectrum. The first oscillator corresponds to the transition from valence band (VB) to Ce 4f states, whereas the second oscillator corresponds to the transition from VB to lower lying Ce 5d band [37,38]. By direct comparison of the experimental data with fitted curves it is obvious that TL model failed to describe adequately behavior of $\langle \varepsilon_2(E) \rangle$ of our samples in the region bellow the band gap. The discrepancy between experimental and numerical data originates from the fact that TL model is based on the assumption that $\varepsilon_2(E)$ vanishes below the band

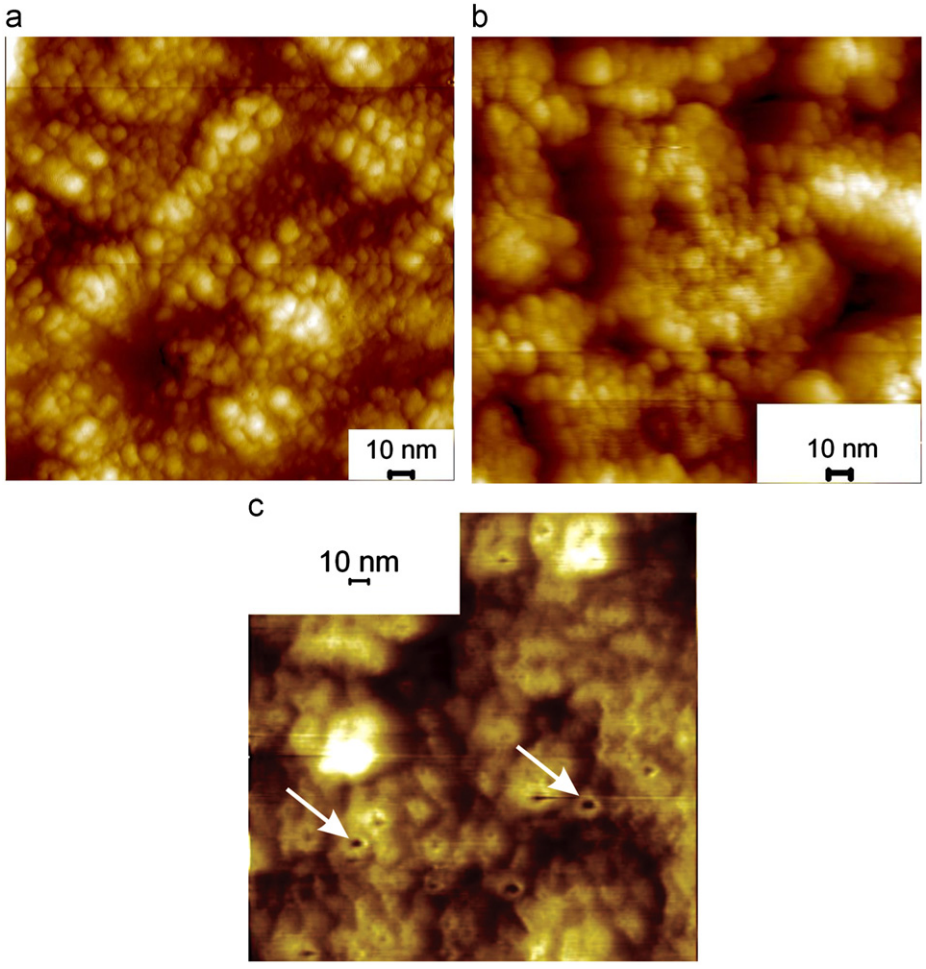

Fig. 3. NC-AFM images of (a) pure, (b) 3 mol% Fe and (c) 5 mol% Fe doped samples.

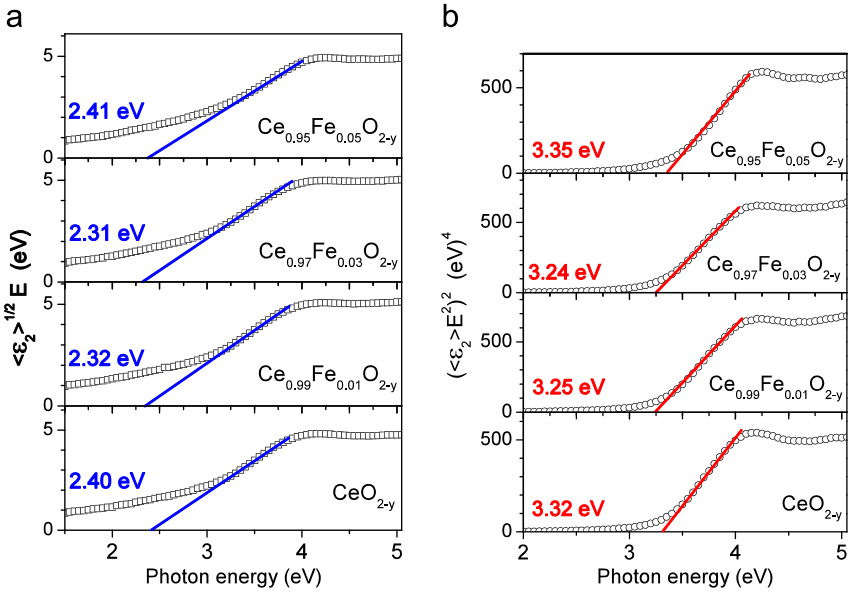

Fig. 4. Tauc plots versus photon energy for (a) indirect (open squares) and (b) direct (open circles) band gap transitions together with linear fits (solid lines), using the Eqs. (2a) and (2b), for pure and Fe^{3+}-doped ceria nanopowders.

gap and this is not valid for our samples. On the other side, as a consequence of this assumption, TL model always gives underestimated band gap values [28].

In nanomaterials, the appearance of defect/disordered states manifests as the non-vanishing absorption in the region bellow the band gap (Urbach tail region) which can be well

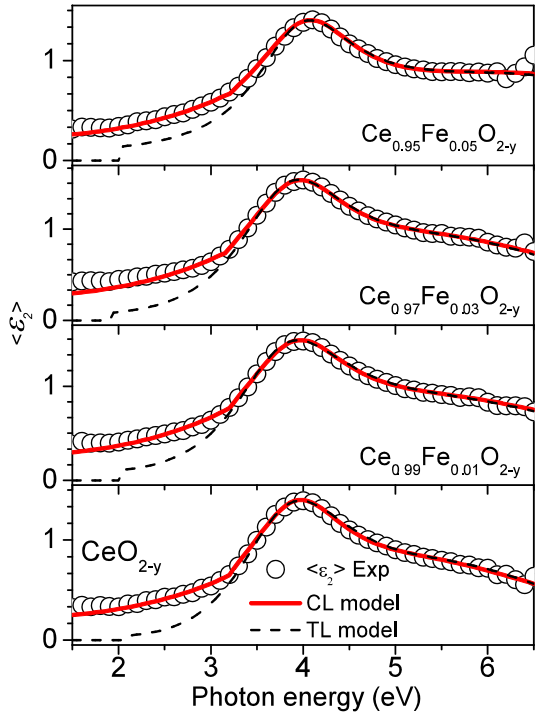

Fig. 5. Imaginary part of pseudo-dielectric function (open symbols) together with numerical fits using Tauc–Lorentz (dashed line) and Cody–Lorentz (full line) model.

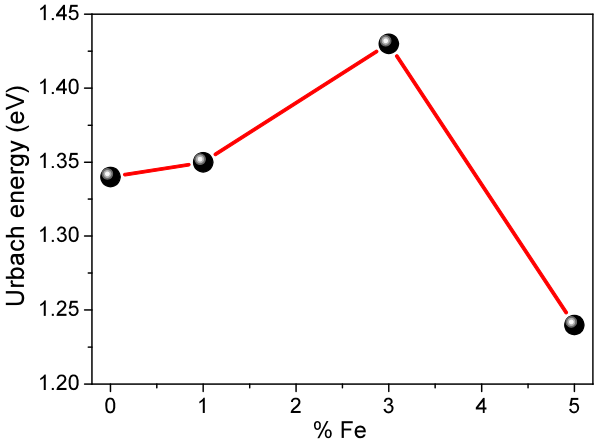

Fig. 6. Variation of Urbach energy in $Ce_{1-x}Fe_xO_{2-y}$ nanopowders.

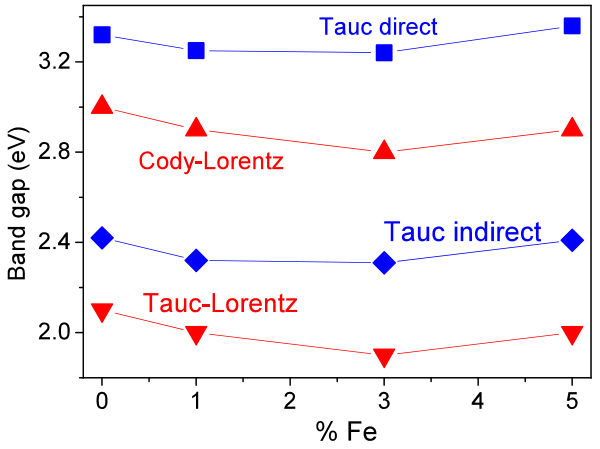

Fig. 7. Band gap variation in pure and Fe^{3+}-doped ceria nanopowders determined from Tauc law, Tauc–Lorentz and Cody–Lorentz models.

described with Urbach rule [39–41]. Nonstoichiometric, nanocrystalline CeO_{2-y} has a lot of oxygen vacancies especially at the nanoparticle surface. The oxygen defects can form localized states inside the band gap [42] affecting the CeO_{2-y} band gap structure [19]. Patsalas et al. [16] suggested that the Urbach absorption tails in ceria nanoparticles originate from oxygen vacancy defect states. Therefore, we decided to apply CL model which can present significantly improved description of $\langle \varepsilon_2(E) \rangle$ in the below-band gap region compared to previous models. To the best of our knowledge, this model is for the first time applied in the band gap study of defective ceria nanoparticles. The fits based on CL model using Eq. (6) are presented with full lines in Fig. 5, using two oscillators as in the case of TL model. It is obvious that by using CL model, we have obtained very good agreement with experimental spectra in the whole measured region. From the fitting procedure we were able to obtain the values of the Urbach and the band gap energies.

In Fig. 6 is presented the variation of Urbach energy (E_u) in pure and Fe-doped ceria samples derived from CL model. From the observed variation, we can see that with Fe doping up to 3 mol%, Urbach energy increases due to the formation of additional localized states inside the band gap. For 5 mol% Fe^{3+}-doped sample the value of E_u decreases. Obtained results are in very good agreement with the Raman spectroscopy measurements from which we have observed increased concentration of oxygen vacancies in the samples with Fe content up to 3 mol% (Fig. 2(c)) after which the phase separation started and the oxygen vacancy concentration decreased.

The variation of the band gap values of $Ce_{1-x}Fe_xO_{2-y}$ ($0 \le x \le 0.05$) nanocrystals, obtained from different SE models, is presented in Fig. 7. As can be seen from Fig. 7, the values of E_g differ significantly among applied models but have a same trend with Fe^{3+} doping. Although XRD data confirmed that CeO_{2-y} nanocrystals are small, the band gap values estimated from different models are lower than for bulk CeO_2 sample, contrary to the quantum confinement model predictions. This fact points out that the dominant role in the band gap behavior of CeO_{2-y} nanocrystals comes from the oxygen defect states formed in the band gap [16].

As we have already discussed, Tauc law yields slightly overestimated values in ellipsometry measurements for both kinds of band gap transitions. The band gap values, calculated from TL model, of $Ce_{1-x}Fe_xO_{2-y}$ samples, have the lowest values and are close to the Tauc band gap values for indirect gap. These underestimated values of band gap were expected because of the fundamental limitations of this model in the region below the band gap. Fitting procedure using Cody–Lorentz model gave the best agreement with experimental data by taking into account the existence of

Urbach absorption tails which originate from defect and disorder states. Having in mind that Tauc law gives overestimated direct band gap values it can be concluded that the band gap values for $Ce_{1-x}Fe_xO_{2-y}$ samples, obtained from CL model, are much closer to the Tauc values for direct band gap transition than to the indirect ones.

From this study we have concluded that the CL model best describes the absorption onset of defective nanocrystalline CeO_{2-y}.

From Fig. 7, we can see that with increasing Fe content, the band gap value further decreases up to 3 mol% of Fe dopant and then slightly increases. The decreasing trend of E_g with Fe^{3+}-doping can be ascribed to the formation of additional defect (localized) states within the band gap. The value of Urbach energy represents the energy width of the localized states. With iron doping, the tails of defect states expand more into the band gap (increase of Urbach energy in Fig. 6) causing the observed decrease of E_g, in agreement with previous studies [43,44]. When the phase separation took place, the band gap slightly increased similarly to the findings of other authors [43]. The higher value of E_g in the 5 mol% Fe^{3+}-doped sample compared to pure CeO_{2-y} can be explained in terms of quantum size effects which now influence more the absorption onset than defect states or by the Burstein–Moss effect [45]. Namely, from XRD data it has been shown that the average crystallite size in this sample is much smaller than in pure CeO_{2-y} sample whereas the Raman measurements and Urbach energy behavior confirmed that this sample has less defective structure.

For moderate Fe dopant concentrations (3 mol% and less), it is possible to induce a shift of optical absorption edge in CeO_{2-y} nanocrystals towards the visible spectral range making this material suitable for application in advanced technologies such as photocatalysis by solar light.

5. Conclusion

The hydrothermal method has been employed to synthesize ceria nanopowders doped with iron. XRD analysis showed that all investigated samples have fluorite cubic crystal structure with particle size in nanometric range, confirmed by NC-AFM results. From Raman spectroscopy measurements we have observed an increase of oxygen vacancies concentration with increasing amount of Fe up to 3 mol%. In the Raman spectrum of $Ce_{0.95}Fe_{0.05}O_{2-y}$ sample, the formation of iron oxide wüstite (FeO) phase was observed.

Using different SE models like Tauc, Tauc–Lorentz and Cody–Lorentz models, we have analyzed the fundamental optical band gap behavior of pure and Fe^{3+}-doped CeO_{2-y} samples. Among all applied models the best agreement between theoretical and experimental data was obtained using the Cody–Lorentz model. Cody–Lorentz model, applied for the first time in the analysis of ceria defective structure, successfully described the existence of Urbach absorption tails due to the presence of oxygen defect states in ceria lattice. The Fe doping of ceria (up to 3 mol%) increases the defect concentration in ceria lattice and shifts the optical absorption edge towards visible spectral range.

Acknowledgment

This work was financially supported by the Serbian Ministry of Education and Science under the Projects ON171032 and III45018, Swiss National Science Foundation through Grant IZ73Z0-128169 and Serbian-Spanish bilateral project through Grant AIB2010SE-00160.

References

[1] R.G. Bamwenda, T. Uesigi, Y. Abe, K. Sayama, H. Arakawa, The photocatalytic oxidation of water to O_2 over pure CeO_2, WO_3, and TiO_2 using Fe^{3+} and Ce^{4+} as electron acceptors, Applied Catalysis B 205 (2001) 117–128.

[2] C. Mao, Y. Zhao, X. Qiu, J. Zhu, C. Burda, Synthesis, characterization and computational study of nitrogen-doped CeO_2 nanoparticles with visible-light activity, Physical Chemistry Chemical Physics 10 (2008) 5633–5638.

[3] L. Yue, X.-M. Zhang, Structural characterization and photocatalytic behaviors of doped CeO_2 nanoparticles, Journal of Alloys and Compounds 475 (2009) 702–705.

[4] Y. Zhai, S. Zhang, H. Pang, Preparation, characterization and photocatalytic activity of CeO_2 nanocrystalline using ammonium bicarbonate as precipitant, Materials Letters 61 (2007) 1863–1866.

[5] P. Ji, J. Zhang, F. Chen, M. Anpo, Study of adsorption and degradation of acid orange 7 on the surface of CeO_2 under visible light irradiation, Applied Catalysis B 85 (2009) 148–154.

[6] O.H. Laguna, M.A. Centeno, M. Boutonnet, J.A. Odriozola, Fe-doped ceria solids synthesized by the microemulsion method for CO oxidation reactions, Applied Catalysis B 106 (2011) 621–629.

[7] Laurianne Truffault, Q.W. Yao, David Wexler, Ivan P. Nevirkovets, Konstantin Konstantinov, Thierry Devers, Sharon Nightingale, Synthesis and characterization of Fe doped CeO_2 nanoparticles for pigmented ultraviolet filter applications, Journal for Nanoscience and Nanotechnology 11 (2011) 4019.

[8] S. Guo, H. Arwin, S.N. Jacobsen, K. Järrendahl, U. Helmersson, A spectroscopic–ellipsometry study of cerium dioxide thin films grown on sapphire by rf magnetron sputtering, Journal of Applied Physics 77 (1995) 5369–5376.

[9] I. Kosacki, H.U. Anderson, Microstructure-property relationships in nanocrystalline oxide thin films, Ionics 6 (2000) 294–311.

[10] X.-H. Liao, J.-M. Zhu, J.-J. Zhu, J.-Z. Xua, H.-Y. Chen, Preparation of monodispersed nanocrystalline CeO_2 powders by microwave irradiation, Chemical Communications (2001) 937–938.

[11] C. Ho, J.C. Yu, T. Kwong, A.C. Mak, S. Lai, Morphology-controllable synthesis of mesoporous CeO_2 nano- and microstructures, Chemistry of Materials 17 (2005) 4514–4522.

[12] C. Mansilla, Structure, microstructure and optical properties of cerium oxide thin films prepared by electron beam evaporation assisted with ion beams, Solid State Sciences 11 (2009) 1456–1464.

[13] R.M. Buenno, J.M. Martinez-Duart, M. Hernández-Vélez, L. Vázquez, Optical and structural characterization of r.f. sputtered CeO_2 thin films, Journal of Materials Science 32 (1997) 1861–1865.

[14] A. Hartridge, M. Ghanashyam Krishna, A.K. Bhattacharya, Optical constants of nanocrystalline lanthanide-doped ceria thin films with the fluorite structure, Journal of Physics and Chemistry of Solids 59 (1998) 859–866.

[15] D. Barreca, G. Bruno, A. Gasparotto, M. Losurdo, E. Tondello, Journal of Materials Science and Engineering 23 (2003) 1013–1016.

[16] P. Patsalas, S. Logothetidis, L. Sygellou, S. Kennou, Structure-dependent electronic properties of nanocrystalline cerium oxide films, Physical Review B 68 (2003) 035104-1–035104-13.
[17] M.Y. Chen, X.T. Zua, X. Xiang, H.L. Zhang, Effects of ion irradiation and annealing on optical and structural properties of CeO_2 films on sapphire, Physica B 389 (2007) 263–268.
[18] A. Pfau, K.D. Schierbaum, The electronic structure of stoichiometric and reduced CeO_2 surfaces: an XPS, UPS and HREELS study, Surface Science 321 (1994) 71–80.
[19] J.-F. Jerratsch, X. Shao, N. Nilius, H.-J. Freund, C. Popa, M.V. Ganduglia-Pirovano, A.M. Burow, J. Sauer, Electron localization in defective ceria films: a study with scanning-tunneling microscopy and density-functional theory, Physical Review Letters 106 (2011) 246801-1–246801-4.
[20] S.V. Gaponenko, Optical Properties of Semiconductor Nanocrystals, Cambridge University press, Cambridge, England, 1998.
[21] Feng Zhang, Peng Wang, J. Koberstein, S. Khalid, Siu-Wai Chan, Cerium oxidation state in ceria nanoparticles and absorption near edge spectroscopy, Surface Science 563 (2004) 74–82.
[22] J.R. McBride, K.C. Hass, B.D. Poindexter, W.H. Weber, Raman and X-ray studies of $Ce_{1-x}RE_xO_{2-y}$, where RE=La, Pr, Nd, Eu, Gd, and Tb, Journal of Applied Physics 76 (1994) 2435–2441.
[23] M. Radović, Z.D. Dohčević-Mitrović, A. Golubović, B. Matović, M. Šćepanović, Z.V. Popović, Hydrothermal synthesis of CeO_2 and $Ce_{0.9}Fe_{0.1}O_2$ nanocrystals, Acta Physica Polonica A 116 (2009) 614–617.
[24] H. Fujiwara, Spectroscopic Ellipsometry Principles and Applications, John Wiley and Sons Ltd., Chichester, England, 2003.
[25] J. Tauc, R. Grigrovici, A. Vancu, Optical properties and electronic structure of amorphous germanium, Physica Status Solidi 15 (1966) 627–637.
[26] G.E. Jellison, F.A. Modine, Parameterization of the optical functions of amorphous materials in the interband region, Applied Physics Letters 69 (1996) 371–373.
[27] G.D. Cody, C.R. Wronski, B. Abeles, R.B. Stephens, B. Brooks, Optical characterization of amorphous slicon hydride films, Solar Cells 2 (1980) 227–243.
[28] A.S. Ferlauto, G.M. Ferreira, J.M. Pearce, C.R. Wronski, R.W. Collins, X.M. Deng, G. Ganguly, Analytical model for the optical functions of amorphous semiconductors from near-infrared to ultraviolet: applications in thin film photovoltaics, Journal of Applied Physics 92 (2002) 2424–2436.
[29] F. Urbach, The long wavelength edge of photographic sensitivity and of the electronic absorption of solids, Physical Review 92 (1953) 1324.
[30] G.K. Williamson, W. Hall, X-ray line broadening from filed aluminium and wolfram, Acta Metallurgica 1 (1953) 22–31.
[31] M.H. Brooker, O. Faurskov Nielsen, E. Praestgaard, Assesment correction procedures for reduction of Raman spectra, Journal of Raman Spectroscopy 25 (1994) 849–854.
[32] Z.D. Dohčević-Mitrović, M.J. Šćepanović, M.U. Grujić-Brojčin, Z.V. Popović, S.B. Bošković, B.M. Matović, M.V. Zinkevich, F. Aldinger, The size and strain effects on the Raman spectra of $Ce_{1-x}Nd_xO_{2-\delta}$ ($0<x<0.25$) nanopowders, Solid State Communications 137 (2006) 387–390.
[33] Z.D. Dohčević-Mitrović, N. Paunović, M. Radović, Z.V. Popović, B. Matović, B. Cekić, V. Ivanovski, Valence state dependent room-temperature ferromagnetism in Fe-doped ceria nanocrystals, Applied Physics Letters 96 (2010) 203104-1–203104-3.
[34] Z.V. Popović, Z.D. Dohčević-Mitrović, N. Paunović, M. Radović, Evidence of charge delocalization in $Ce_{1-x}Fe_x^{2+(3+)}O_{2-y}$ nanocrystals (x=0, 0.06, 0.12), Physical Review B 85 (2012) 014302-1–014302-6.
[35] D.L.A. de Faria, S. Venâncio Silva, M.T. de Oliveira, Raman microspectroscopy of some iron oxides and oxyhydroxides, Journal of Raman Spectroscopy 28 (1997) 873–878.
[36] T. Ichiia, T. Fukuma, K. Kobayashi, H. Yamada, K. Matsushige, Phase-separated alkanethiol self-assembled monolayers investigated by non-contact AFM, Applied Surface Science 210 (2003) 99–104.
[37] N.V. Skorodumova, R. Ahuja, S. Simak, A. Abrikosov, B. Johansson, B. Lundqvist, Electronic, bonding and optical properties of CeO_2 and Ce_2O_3 from first principals, Physical Review B 64 (2001) 115108-1–115108-9.
[38] M. Marabelli, P. Wachter, Covalent insulator CeO_2: optical reflectivity measurements, Physical Review B 36 (1987) 1238–1243.
[39] G. Sinha, K. Adhikary, S. Chaudhuri, Optical properties of nanocrystalline α-GaO(OH) thin films, Journal of Physics: Condensed Matter 18 (2006) 2409–2415.
[40] J.J. Glennon, R. Tang, W.E. Buhro, R.A. Loomis, Exciton localization and migration in individual CdSe quantum wires at low temperatures, Physical Review B 80 (2009) 081303-1–081303-4.
[41] Z.D. Dohčević-Mitrović, A. Milutinović, D. Popović, D. Vasiljević-Radović, Z.V. Popović, Variable energy gap of SiCN nanopowders, Applied Physics A 84 (2006) 197–202.
[42] T. Kamiya, K. Nomura, M. Hirano, H. Hosono, Electronic structure of oxygen deficient amorphous oxide semiconductor a-$InGaZnO_{4-x}$: optical analyses and first-principle calculations, Physica Status Solidi C 5 (2008) 3098–3100.
[43] P.C.A. Brito, D.A.A. Santos, J. Gerivaldo, S. Duque, M.A. Macêdo, Structural and magnetic study of Fe-doped CeO_2, Physica B 405 (2010) 1821–1825.
[44] T. Dhannia, S. Jayalekshmi, M.C.Santhosh Kumar, T.Prasada Rao, A.Chandra Bose, Effect of iron doping and annealing on structural and optical properties of cerium oxide nanocrystals, Journal of Physics and Chemistry of Solids 71 (2010) 1020.
[45] I. Hamberg, C.G. Granqvist, K.-F. Berggren, B.E. Sernelius, L. Engstrom, Band-gap widening in heavily Sn-doped In_2O_3, Physical Review B 30 (1984) 3240–3249.